nature cities

Article

https://doi.org/10.1038/s44284-024-00047-3

Optimizing retro-reflective surfaces to untrap radiation and cool cities

Received: 27 August 2023

Accepted: 13 February 2024

Published online: 11 March 2024

Check for updates

Xinjie Huang[1], Elie Bou-Zeid[1] ✉, Ilaria Pigliautile[2,3], Anna Laura Pisello[2,3] & Jyotirmoy Mandal[1]

Extreme heat and its various impacts are a growing threat to cities and their residents, and it is increasingly clear that portfolios of solutions are needed to mitigate the resulting risks. Here we comprehensively evaluate and optimize the application of existing retro-reflective (RR) materials, which reflect incoming solar radiation back to the sky, on urban surfaces to cool them. Using detailed energy budget models, we show that RR walls and pavements decrease urban canyon surface temperatures by up to 20 °C and canyon air temperatures by up to 2.6 °C, outperforming highly reflective surfaces, with a notable improvement in pedestrian thermal comfort (up to 0.55 °C and 153 W m^{-2} reductions in human skin temperature and net radiative gain, respectively). We then develop optimized RR design guidelines for diverse climatic conditions, latitudes, seasons and urban geometries. On the basis of our analysis, we recommend RR pavements for open, low-rise areas and propose specific RR wall design strategies for compact, high-rise areas.

Rapid urbanization replaces natural land covers with surfaces and structures that often have lower solar reflectance (albedo) and higher heat storage capacity, causing them to absorb and retain more solar energy. These environmental modifications profoundly alter surface energy and water budgets over urban terrains, ultimately affecting urban microclimatic conditions, with the urban heat island (UHI) phenomenon being the most well-known consequence. The UHI effect, manifested as higher air and surface temperatures in urban areas compared with those in adjacent non-urban areas[1], exacerbates thermal stress especially during extreme heat events under global climate change. This synergistic interaction will result in surging heat-related morbidity and mortality in urban settings[2,3]. To curb the lethal urban overheating problem, numerous urban heat reduction strategies have been proposed, evaluated and implemented, including gray (for example, highly reflective (HR) roofs, photovoltaic surfaces, advanced air-conditioning systems), green (for example, lawns, trees, green roofs) and blue (for example, urban lakes, irrigation, misting) infrastructure.

HR surfaces, also known as reflective, cool and high-albedo surfaces, are some of the most extensively studied strategies and have been shown to be a promising and increasingly adopted approach[4,5]. As shown in the contrasting schematics of normal (Fig. 1a) and HR (Fig. 1b) surfaces, HR roofs feature high solar reflectance (albedo) that can raise the fraction of incident sunlight returned to outer space, thus reducing the amount absorbed by building surfaces. In recent years, HR roofs and pavements have been implemented in many cities around the world, for example, as part of the Global Cool Cities Alliance (https://globalcoolcities.org/), and they are increasingly adopted in authoritative building standards (for example, The American Society of Heating, Refrigerating and Air-Conditioning Engineers[6]) and large-scale governmental campaigns (for example, Los Angeles[7] and Phoenix[8]). Although proven to be generally beneficial, especially in roof applications in hot, low-rise, low-density urban areas, the façade and ground application of HR surfaces pose multiple problems, including glare and intense diffuse reflection of energy onto neighboring buildings, pavements and pedestrians. This can aggravate pedestrian-level thermal stress[9,10]. In addition, roof cooling by HR surfaces is useful at the city scale but may have only indirect and potentially weak influence on street-level and canyon conditions[11], which are the most relevant for health and livability outcomes.

[1]Department of Civil and Environmental Engineering, Princeton University, Princeton, NJ, USA. [2]CIRIAF - Interuniversity Research Center, University of Perugia, Perugia, Italy. [3]Department of Engineering, University of Perugia, Perugia, Italy. ✉e-mail: ebouzeid@princeton.edu

https://doi.org/10.1038/s44284-024-00047-3

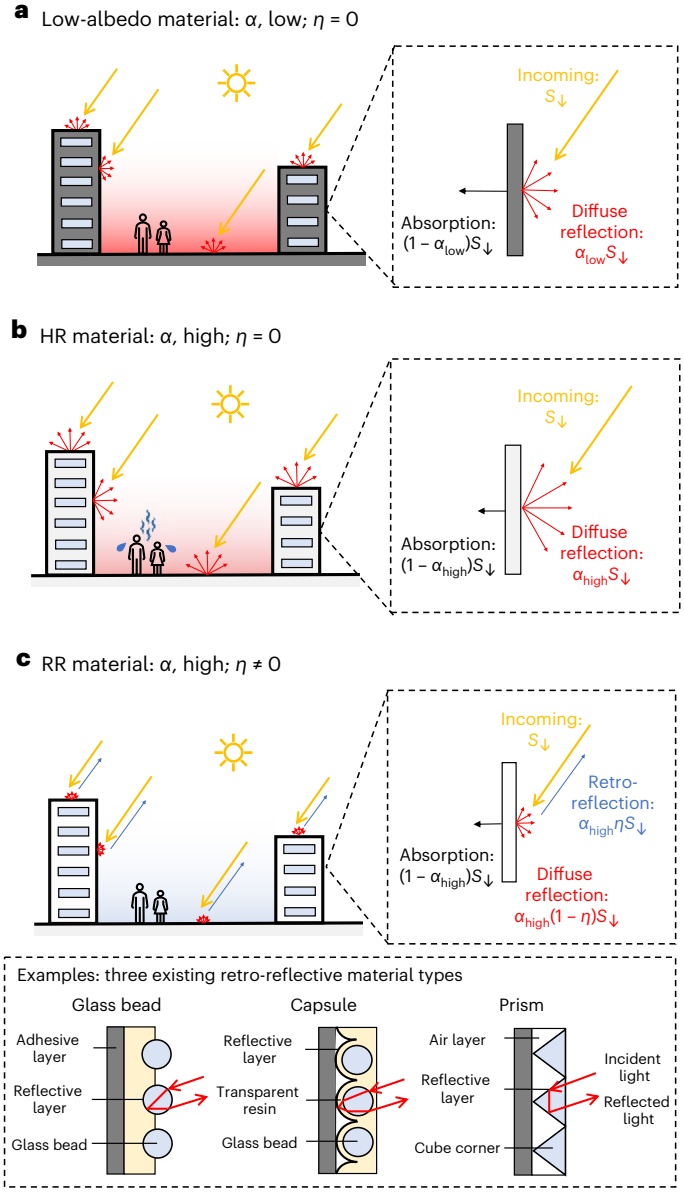

Fig. 1 | Total reflectance and retro-reflectance of three surfaces in urban environments. a–**c**, Schematics of normal (low-albedo) (**a**), HR (**b**) and RR (**c**) surfaces in urban environments. Three examples of common RR material types are shown in **c**. $SW_{\downarrow}$, downwelling shortwave radiation; α, total reflectivity, that is, albedo; η, retro-reflectivity.

To cool the canyon air and pedestrians therein, various UHI abatement solutions and technologies have been proposed. These include retro-reflective (RR)[12–14], thermochromic[15,16] and radiative cooling[17,18] materials. Among these promising technologies, RR surfaces, which can reflect a fraction of the incoming sunlight directly back to its source (ideally) or at least upwards (imperfectly) (Fig. 1c), show great potential to overcome some of the disadvantages of HR surfaces and provide additional cooling benefits. RR materials are widely used in the transportation industry with relatively mature manufacturing technology. Despite an increasing number of studies on their application to building surfaces, most previous experimental studies have focused on optical properties (for example, total reflectivity, retro-reflectivity and angular characteristics)[19–21], and most previous modeling studies have focused on shortwave radiation analysis[12,22,23]. However, the dynamic coupling of RR surfaces and façades to a realistic urban microclimate model, which is critical for understanding their real-world benefits, remains lacking.

Such a coupled model is required to provide a comprehensive assessment of RR cooling performance. Previous studies on RR surfaces have reported a wide range of urban reflectivity increases (3–36%)[13,24,25], urban surface temperature reduction (−0.4 °C to −25 °C)[26–28] and indoor air temperature reduction (−2.4 °C to −7.7 °C, using RR windows)[29,30]. The effectiveness of these RR benefits depends strongly on material types, surface selection, local climate and weather conditions, street geometries and orientations, among other factors. Thus, it is imperative to comprehensively evaluate RR cooling performance across the whole parameter space, as well as link the benefits more directly to human thermal comfort. This will allow an optimized design strategy, which will be essential to ensure broader applicability and efficient implementation of this promising urban cooling technique.

To bridge the aforementioned gaps, we developed a new RR module and embedded it in a comprehensive urban canopy model (UCM). UCMs are very broadly used urban land surface modeling frameworks in urban climate applications: they have been extensively used to simulate urban surface energy fluxes and meteorology at local, regional and global scales[31–34]. Specifically, the UCM used in this study was developed at Princeton University (PUCM)[35–39]. The PUCM represents a generic infinitely long two-dimensional street canyon as the basic urban surface unit, which consists of a roof, two facing walls and a ground surface. It has been successfully validated under various climates, demonstrating good predictive capabilities along with high computational efficiency. In addition, a human thermal comfort model has been recently coupled into the PUCM: it dynamically resolves radiative, convective, conductive and evaporative heat exchanges between a pedestrian and their surrounding urban environment to more realistically represent human-level heat stress. Thus, the PUCM is well suited to assess the cascade of impacts of RR surfaces on street canyon air and surfaces and pedestrians in various urban densities and latitudes. The UCM framework, RR surface representation and numerical experiment design are described in Methods.

The roadmap of the whole study is shown in Supplementary Fig. 1. Using the PUCM-RR model, we first conduct a local evaluation of the impacts of RR walls and pavements on UHI abatement and human thermal comfort improvement, with a particular focus on investigating the significance of two key optical properties (that is, total and retro-reflectivity) for common RR material types. Next, we investigate the optimal implementation strategy of RR by testing different latitudes, seasons, street geometries and orientations, considering both solar radiation exposure levels across various geographic regions and solar radiation distribution schemes in diverse street configurations. Through these approaches, we develop globally informative design guidelines for RR surfaces tailored to localized conditions, which can facilitate the effective implementation of RR materials to address the widespread urban overheating problem.

Results

Enhanced cooling with synergistic reflective benefits

The cooling effects of RR materials on urban canyon surface and air temperatures were assessed for diverse RR material types applied to urban façades and grounds. We first tested various combinations of total reflectivity and retro-reflectivity in their common ranges (0.3–0.9 and 0–0.5, respectively) set based on three typical RR types. Here the total reflectivity α is the fraction of incoming shortwave radiation that is reflected in any direction (that is, albedo), while retro-reflectivity η is the fraction of the total reflected radiation that is directed in the same direction from which it came (the other fraction is assumed to be completely diffuse).

As presented in Supplementary Table 1, we tested normal walls + ground (baseline scenario), RR walls (that is, RR walls + normal ground; Fig. 2a,c) and RR grounds (that is, RR grounds + normal walls; Fig. 2b,d) separately. The cooling effects (ΔT_W, ΔT_G and ΔT_{can} for wall, ground and canyon air temperatures, respectively) were evaluated by

https://doi.org/10.1038/s44284-024-00047-3

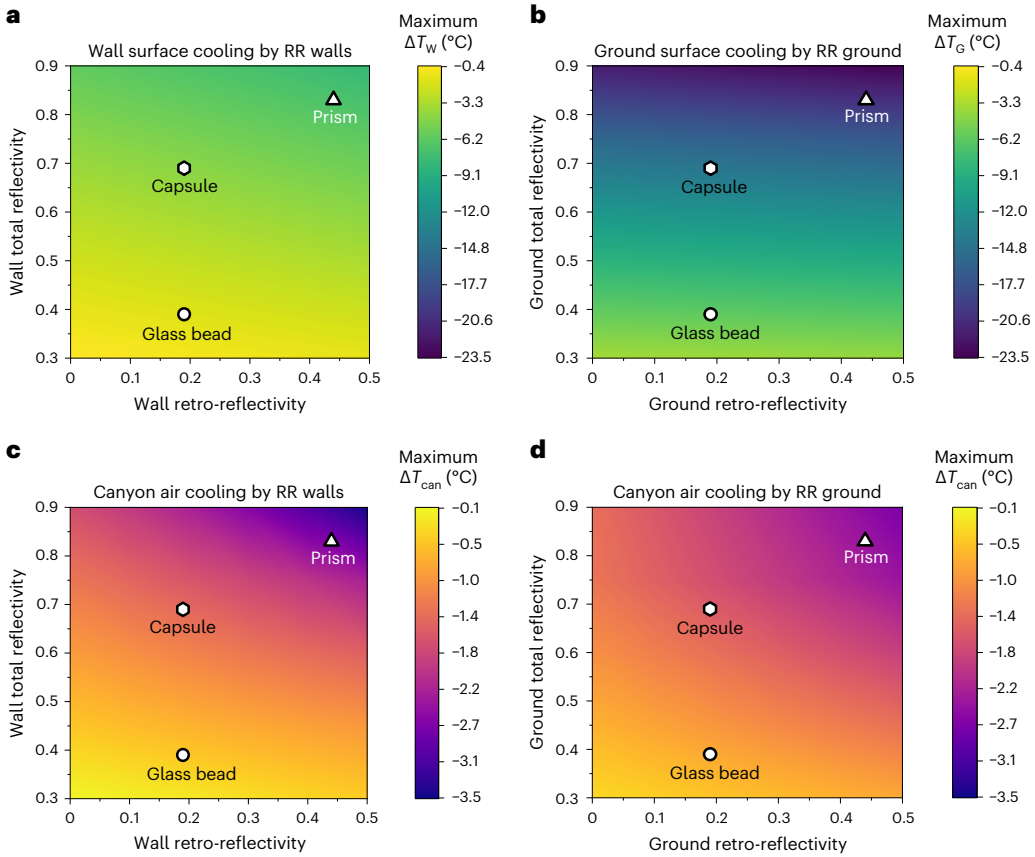

Fig. 2 | Maximum surface temperature reductions and maximum canyon air temperature reductions by RR walls and RR ground. a–d, Wall surface cooling (maximum ΔT_W) by RR walls (**a**), ground surface cooling (maximum ΔT_G) by RR ground (**b**) and canyon air cooling (maximum ΔT_{can}) by RR walls (**c**) and RR ground (**d**) with different total reflectivity and retro-reflectivity.

comparing the RR wall or ground scenarios with the normal baseline scenarios. The scenarios were tested on a hot summer day (7 July) in 2010, with meteorological forcing (air temperature and relative humidity, wind speed above the canyon and incoming longwave radiation; Supplementary Fig. 2) and urban settings based on Princeton, NJ, USA, with a canyon aspect ratio (building height/road width) of 1. For incoming shortwave, intermittent cloudiness creates trends that confound our analyses and are not useful or generalizable. Thus, we generated an idealized clear-sky solar radiation diurnal cycle as input (see Methods for details).

Figure 2a,b shows the maximum surface temperature reductions for RR walls ($\Delta T_W = \Delta T_{W,RR} - \Delta T_{W,normal}$) and RR ground ($\Delta T_G = \Delta T_{G,RR} - \Delta T_{G,normal}$), respectively. We found that RR walls can lead to a substantial wall surface cooling benefit of −0.4 °C to −8 °C, and RR ground results in an even greater surface cooling that is largely attributed to the high albedo (with minimal impact of retro-reflectivity). Figure 2c,d shows the maximum canyon air temperature reductions ($\Delta T_{can} = \Delta T_{can,RR} - \Delta T_{can,normal}$) by RR walls and RR ground, respectively. In the test range, RR walls and ground both show an evident cooling effect by reducing urban canyon air temperatures by 0.1–3.5 °C (Fig. 2c) and 0.3–2.7 °C (Fig. 2d), respectively. In Fig. 2, we also show three common types of RR material based on their reference optical properties: prism ($\alpha = 0.83$, $\eta = 0.44$; ref. 40), capsule ($\alpha = 0.69$, $\eta = 0.19$; refs. 41,42) and glass bead ($\alpha = 0.39$, $\eta = 0.19$; ref. 19). Note that these reference values are based on test results from previous studies, while specific values in practice may vary with different manufacturing technologies and material aging. The prism RR material yielded the best performance, resulting in a maximum reduction of −2.6 °C (applied on walls) and −2.5 °C (applied on the ground) in canyon air temperature. These reductions were −2.1 °C and −1.7 °C higher than the least effective type (glass bead). The superior reflectivity properties are associated with the wider effective reflective angle ranges of the prism structure due to multiple total internal reflections occurring within their corner cube geometry. Hereafter, we will mainly use the optimal type (that is, prism) to show the maximum potential cooling benefits of RR materials.

Multi-faceted UHI reduction

To unravel the contribution of each reflectivity to the total cooling effects and to contrast new RR surfaces with conventional HR materials, we compare the following three scenarios with the optical properties of the optimal RR type (prism): (1) highly RR, $\alpha = 0.83$, $\eta = 0.44$; (2) highly diffuse reflective, $\alpha = 0.83$, $\eta = 0$; and (3) normal, $\alpha = 0.25$ for walls and $\alpha = 0.15$ for ground, $\eta = 0$. Comparing scenarios 1 and 2, we can isolate the benefits of retro-reflectivity (green bars in Fig. 3a–c); while comparing scenarios 2 and 3, we can isolate the impacts of total reflectivity (that is, albedo, orange bars in Fig. 3a–c). The sum of the green and orange bars represents the combined effect comparing RR with normal surfaces, which are shown by lines in Fig. 3a–c. Figure 3a–c shows the diurnal profiles of these isolated cooling benefits on canyon air, RR surface and normal surface, with the top and bottom panels denoting the implementation of RR walls (that is, RR walls + normal ground) and RR ground (that is, RR ground + normal walls), respectively.

As shown in Fig. 3a, both RR walls and ground yield substantial cooling for canyon air during the daytime (06:00–20:00) with slight cooling (about −0.5 °C) extending into the nighttime due to a reduction in stored heat that is released from building materials. During the daytime, RR walls are most effective in the early morning (around 08:00) and late afternoon (around 18:00) with low sun angles, while

https://doi.org/10.1038/s44284-024-00047-3

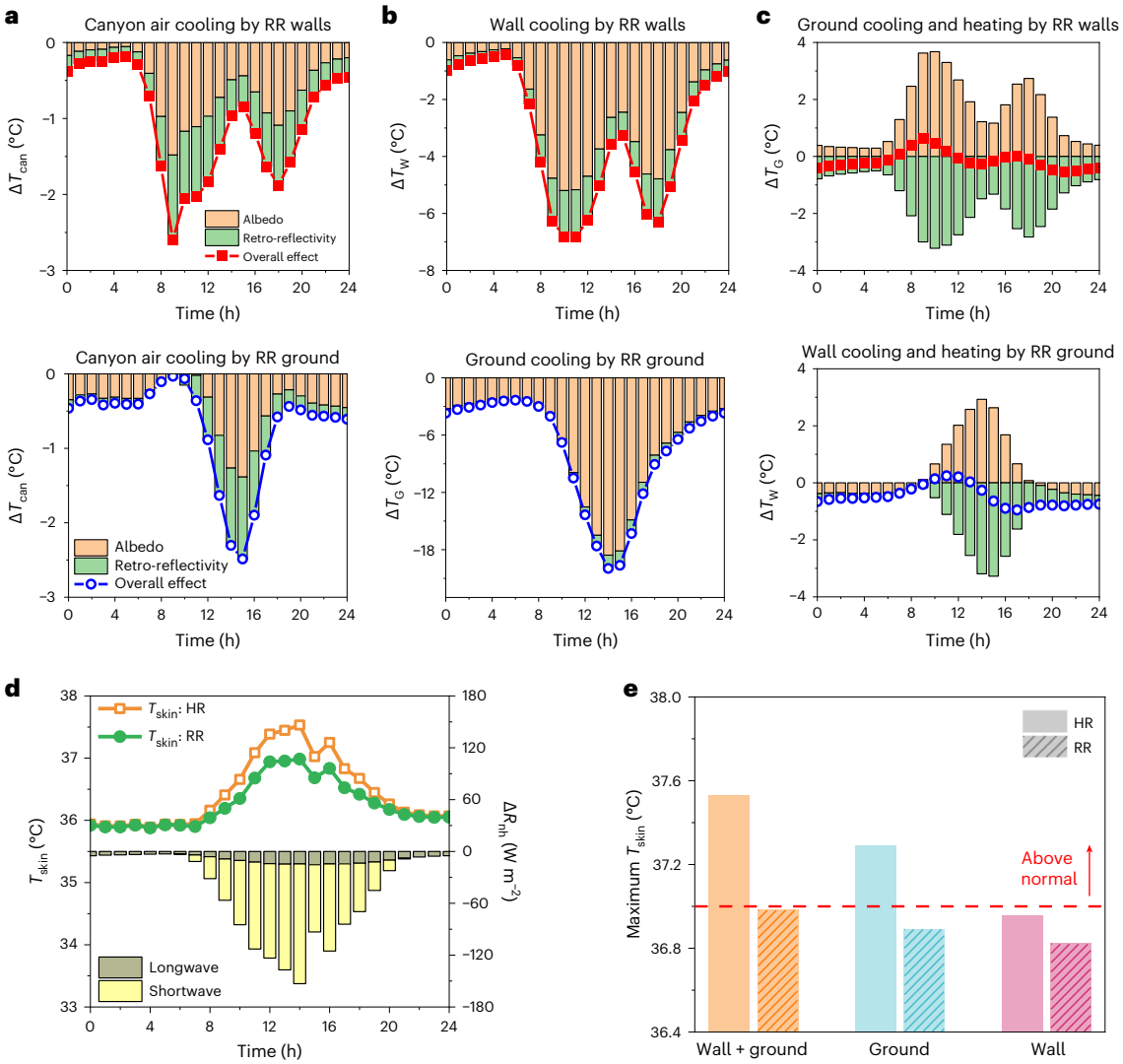

Fig. 3 | Effects of albedo and retro-reflectivity on temperature and thermal comfort in urban canyons. a–**c**, Impacts of albedo and retro-reflectivity of RR surfaces on canyon air temperature (ΔT_{can}) (**a**), RR surface temperature (ΔT_W or ΔT_G) (**b**) and the opposite surface temperature (ΔT_G or ΔT_W) (**c**). The top and bottom panels show cooling effects of RR walls and ground, respectively. **d**, Human skin temperature (T_{skin}) and net human radiation reduction (ΔR_{nh}) for HR and RR walls + ground. **e**, Maximum T_{skin} for HR and RR walls + ground, ground and wall.

RR ground is most effective at noon (12:00–16:00) when the sun hits the ground at near right angles.

Compared with HR surfaces, RR surfaces not only enhance daytime air temperature reduction but also mitigate the adverse effects of high reflection onto the opposite surfaces (which have a much lower overall albedo than the treated surface). As shown by the green bars in Fig. 3a–c, RR surfaces demonstrate manifold temperature reductions for the opposite surface (up to −3.3 °C, through the direct reduction of reflected radiation and feedback from reduced air temperature), the canyon air (up to −1.1 °C, comparing RR with HR surfaces, mainly through opposite surface–air interactions) and the RR surface itself (up to −1.6 °C, through reduced secondary reflection from the opposite surface and air–RR surface interactions). By contrast, HR surfaces would result in unintended temperature increases (up to +3.7 °C) on the opposite surface, as presented by the orange bars in Fig. 3c.

Human thermal comfort enhancement

Direct assessment of human thermal comfort benefits is more informative for evaluating RR surfaces as a cooling strategy than relying solely on surface and air temperature reductions. PUCM-RR features the capability to capture changes in human thermal stress responses (represented as human skin temperature, T_{skin}) and energy exchanges (for example, net human radiation: the sum of net (incoming − outgoing) shortwave and longwave radiation, $R_{nh} = SW_{in} - SW_{out} + LW_{in} - LW_{out}$) induced by different urban environmental variations (see Methods for details). With PUCM-RR, we tested HR and RR walls and grounds, as well as their combination (walls + grounds), to compute the changes in human skin temperature (T_{skin}) and human radiation budget ($\Delta R_{nh} = \Delta R_{nh,RR} - \Delta R_{nh,HR}$). Figure 3d shows the results over a full diurnal cycle for the combination scenario (only-wall and only-ground scenarios are shown in Supplementary Fig. 3), while the maximum human skin temperature reduction for each scenario is shown in Fig. 3e.

As shown in Fig. 3d,e, RR surfaces improve pedestrian thermal comfort by reducing human skin temperatures by up to −0.55 °C compared with HR surfaces, especially during the hottest hours (10:00–16:00). By observing the diurnal profiles of human net radiation changes (gray and yellow bars for longwave and shortwave, respectively, in Fig. 3d), it is clear that shortwave radiation reduction (up to −138 W m^{-2}) plays a dominant role in offsetting the higher reflection from the higher total albedo of RR material on pedestrians, and longwave radiation reduction (up to −15 W m^{-2}) induced by urban surface

https://doi.org/10.1038/s44284-024-00047-3

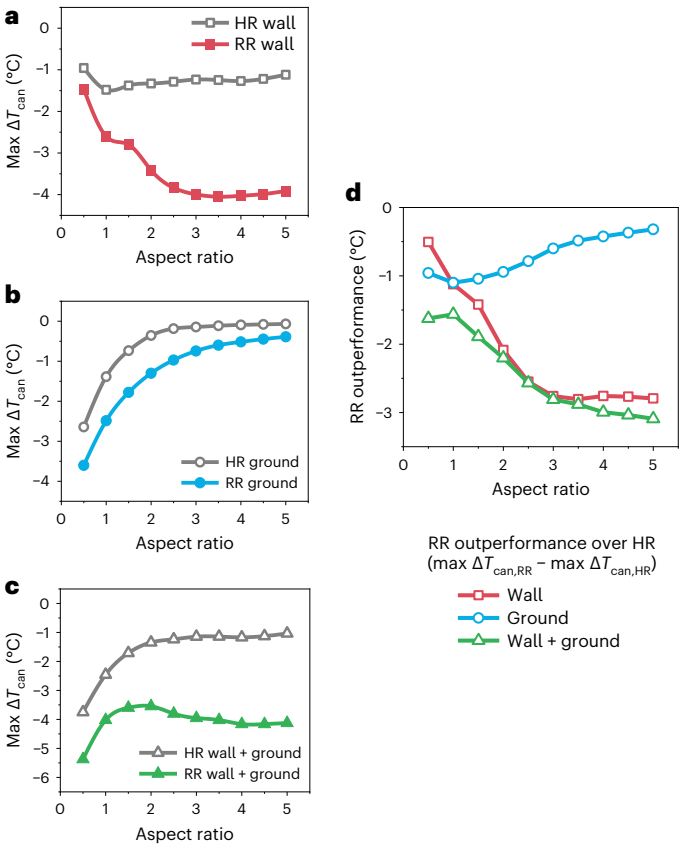

Fig. 4 | Effect of different aspect ratios on the maximum canyon air temperature reduction by HR and RR surfaces. a–d, Changes in the maximum canyon air temperature reduction (maximum ΔT_{can}) with different aspect ratios for both RR and HR wall (**a**), ground (**b**) and wall and ground (**c**) and RR outperformance over HR (maximum $\Delta T_{can,RR}$ − maximum $\Delta T_{can,HR}$) for the three plans (**d**).

temperature reduction shows persistent but minor impacts over the diurnal cycle. Figure 3e shows that compared with HR surfaces, RR surfaces effectively alleviate the reflection-induced heat burden and reduce human skin temperatures below the upper threshold (37 °C) of the normal skin temperature range[43] in all tested scenarios.

Efficient façade selection for different urban geometries

Urban geometry determines the detailed radiative exchanges and distribution among urban surfaces inside a street canyon, affecting the effectiveness of RR surface implementation. To facilitate optimal implementation of RR surfaces considering different street geometries, we tested both HR and RR materials implemented on walls, ground and their combination (walls + ground) in a wide range of aspect ratios from 0.5 to 5.0, with intervals of 0.5. The maximum RR and HR cooling effects of these ten scenarios are shown in Fig. 4.

Cooling performances of RR walls (Fig. 4a) and ground (Fig. 4b) rapidly surge and decay, respectively, at relatively low aspect ratios (from 0.5 to 3.0) and then tend to converge to constant values (−4 °C and −0.4 °C, respectively) at higher aspect ratios (where the buildings are much taller than the street width). Thus, the combination plan (Fig. 4c) shows a non-monotonic variation with aspect ratios: implementing RR walls and ground together shows promising cooling performance of 3.6–5.4 °C for all streets, with the most evident effect at low aspect ratios.

Figure 4a–c shows that RR surfaces outperform HR surfaces in all tested scenarios, and Fig. 4d further shows such outperformance using the differences between maximum cooling effects of these two materials (maximum $\Delta T_{can,RR}$ − maximum $\Delta T_{can,HR}$). For all aspect ratios, the combined RR plan clearly surpasses the combined HR plan by 1.6–3.1 °C. If only one facet is to be retrofitted considering cost-effectiveness, RR walls are particularly recommended for deep street canyons. For low-density or low-rise urban areas, RR walls and ground provide equivalent cooling benefits that only improve moderately on the performance of HR surfaces. In such cases, the lower-cost HR materials may be a sufficient alternative. Note that here we consider uniform building heights within the street canyon, while the cooling effects can be amplified if RR surfaces are implemented on the walls of taller buildings or the roofs of shorter buildings, leveraging the variability in urban building heights.

Strategic application under different solar radiation

Solar radiation incidence on a specific urban surface varies in space (for example, with latitude), in time (for example, season or time of day) and with local street geometry (for example, street orientations). To explore how to leverage RR cooling potentials considering different spatiotemporal solar radiation distribution, we tested normal and RR materials for different latitudes (for 75° N to 75° S with intervals of 15°), months (each 21st day for January to December) and street orientations (north–south, northeast–southwest, east–west and northwest–southeast; see illustrations at the top in Fig. 5). To compare the cooling performance of RR surfaces across various climatic conditions, we present the maximum reduction in street canyon net shortwave radiation ($S_{can} = hS_{W1} + hS_{W2} + wS_G$, where h and w are wall height and street width, respectively) by comparing RR scenarios with normal scenarios (that is, $\Delta S_{can} = S_{can\_RR} - S_{can\_normal}$) in Fig. 5.

As shown in Fig. 5, RR ground is found to be always most effective for low-latitude regions, while RR wall performance highly depends on street orientations. RR ground causes a notable reduction (up to −240 W m^{-2}) in the radiative budget of street canyons at noon, with a wider (from 60° N to 60° S) and narrower (from 30° N to 30° S) effective application range on north–south and east–west oriented streets, respectively. RR walls in north–south streets are basically beneficial for all latitudes and both hemispheres, with evident summertime cooling (up to −135 W m^{-2}) and insignificant wintertime cooling, which is the ideal combination from thermal comfort and energy perspectives. By contrast, RR walls in east–west streets have a more complex impact. RR coatings on north-facing walls in the Northern Hemisphere and south-facing ones in the Southern Hemisphere have a very weak impact on the radiative balance of the canyon. The opposite walls (south-facing in the Northern Hemisphere and north-facing in the Southern Hemisphere) provide cooling benefits at high latitudes, but the benefits decrease more quickly (and the unintended wintertime cooling increases) at mid-latitudes in that hemisphere. In addition, northeast–southwest and northwest–southeast streets show combined spatiotemporal features of the other two orientations. These two diagonal streets show similar maximum canyon shortwave radiation reductions (but at different times) due to symmetrical paths of the Sun.

Global generalized design guidelines

To better enable real-world deployment across cities worldwide, it would be more pragmatic to apply RR materials to specific urban surfaces rather than attempting to cover all facets of an entire city. Therefore, optimal selection of the most effective RR surface is of practical importance. Combining global spatiotemporal solar radiation distribution and various local street geometries, we aim to propose worldwide generalized design guidelines for more effective and efficient RR surface implementation. In this section, we replicated the simulations in the previous section, which used the baseline aspect ratio of 1, for the other three typical aspect ratios: 0.5, 2 and 5.

For the optimization, we used the "maximum canyon shortwave radiation reduction" (that is, maximum ΔS_{can}) in summer (representative days: 21 June, July and August for the Northern Hemisphere; 21 December, January and February for the Southern Hemisphere)

https://doi.org/10.1038/s44284-024-00047-3

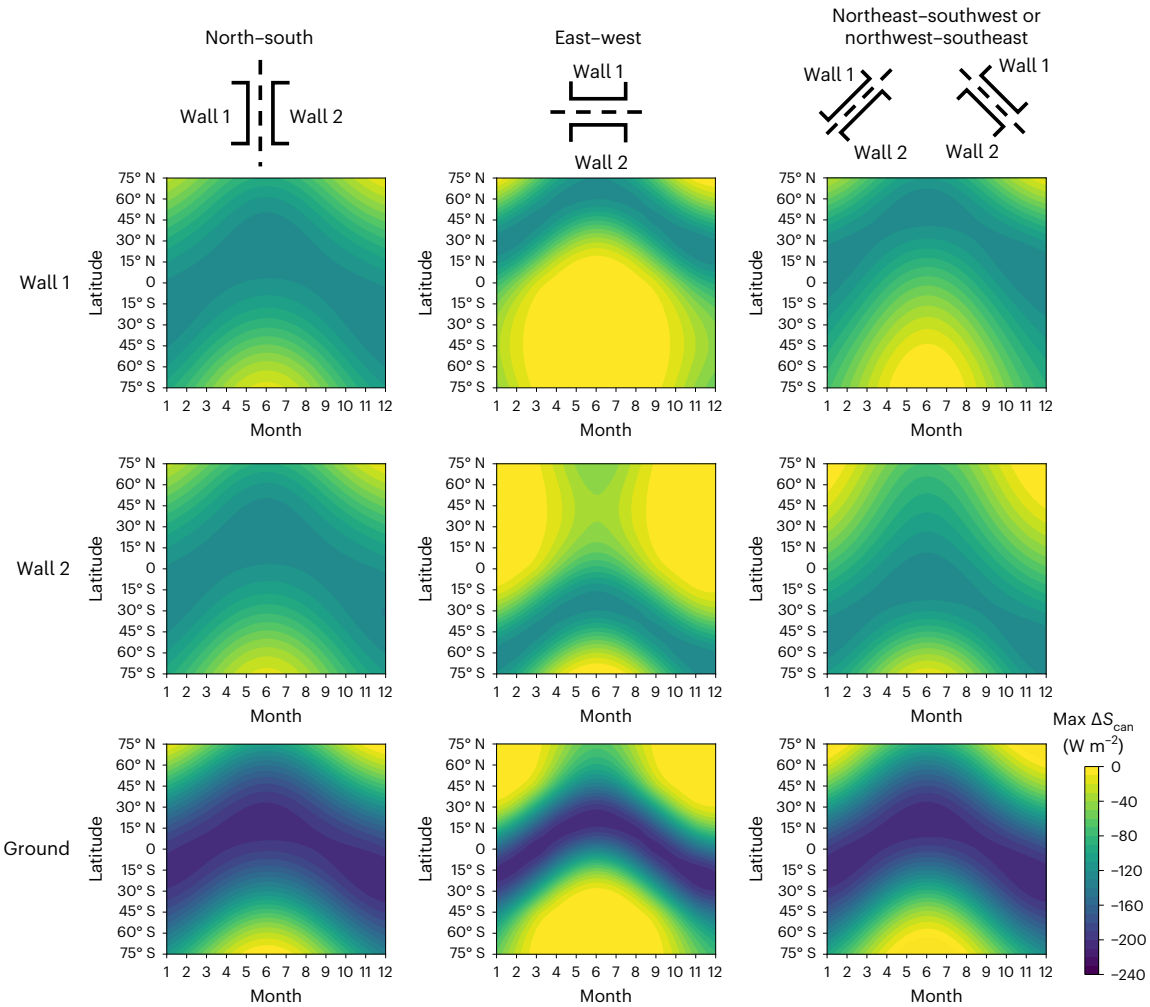

Fig. 5 | Maximum reduction in street canyon net shortwave radiation. Maximum reduction in street canyon (aspect ratio 1) net shortwave radiation (maximum ΔS_{can}) by RR surfaces (wall 1, wall 2 and ground) under different latitudes, months and street orientations.

to identify the most effective RR surface. This optimization criterion directly measures the amount of untrapped radiation by RR surfaces and can be further transferred to many specific heat-related applications (for example, energy, temperature, comfort) by local researchers and practitioners. The single most effective RR surface with greater than 10% difference relative to other surfaces is shown in Fig. 6 with different colors, while multiple most effective RR surfaces are also denoted if insignificant differences (that is, lower than 10%) were found among them.

As shown in Fig. 6, the identification of the most effective RR surfaces is highly dependent on street orientation. North–south streets (Fig. 6a) present the simplest case: the most effective RR surface shifts predominantly according to urban geometries. The ground and walls are clearly favored for low and high aspect ratios, respectively, with negligible differences between the two walls. For east–west and diagonal streets (Fig. 6b,c), the sun path in the sky leads to more complicated results, with the shifting of the most effective RR surfaces at different latitudes. At low aspect ratios (for example, 0.5), the ground is dominantly preferred at all latitudes; with the increase in aspect ratios (for example, at 1 and 2), wall 1 (south-facing) and wall 2 (north-facing) become more advantageous at high latitudes for the Northern and Southern hemispheres, respectively. At the highest aspect ratio of 5, high and low latitudes show different optimization results. For example, in the Northern Hemisphere, south-facing (wall 1) and north-facing (wall 2) are preferred for high and low latitudes, respectively, due to different sun paths. These results for low latitudes are due to the fact that strong insolation of the wall occurs during only the early morning and late afternoon when the sun angle in the sky is low, and the sun path is such that the insolated walls at those times are the north-facing and south-facing ones in the Northern and Southern hemispheres, respectively.

Discussion

We proposed the application of technologically mature RR materials over urban surfaces to tackle the urban overheating challenge by mitigating one of the main drivers of UHI effects: the geometric trapping of radiation in complex and dense urban canopies. Our results quantified the great potential of RR surfaces to provide enhanced cooling benefits and counteract some deficits of traditional HR materials and emphasized the importance of appropriate RR type selection for urban cooling. We revealed that implementing the most effective RR material (prism) on walls and ground decreases urban canyon air temperatures by up to 2.6 °C and 2.5 °C, respectively, and contributes to multi-faceted cooling benefits for other surfaces (up to −3.3 °C) and pedestrians (up to −0.55 °C in skin temperature and −153 W m^{-2} in net radiation compared with HR surfaces).

To facilitate the effective and efficient implementation of RR surfaces, we developed optimal design guidelines for cities worldwide, considering diverse street geometries (for example, aspect ratios and street orientations) and climatic conditions (for example,

https://doi.org/10.1038/s44284-024-00047-3

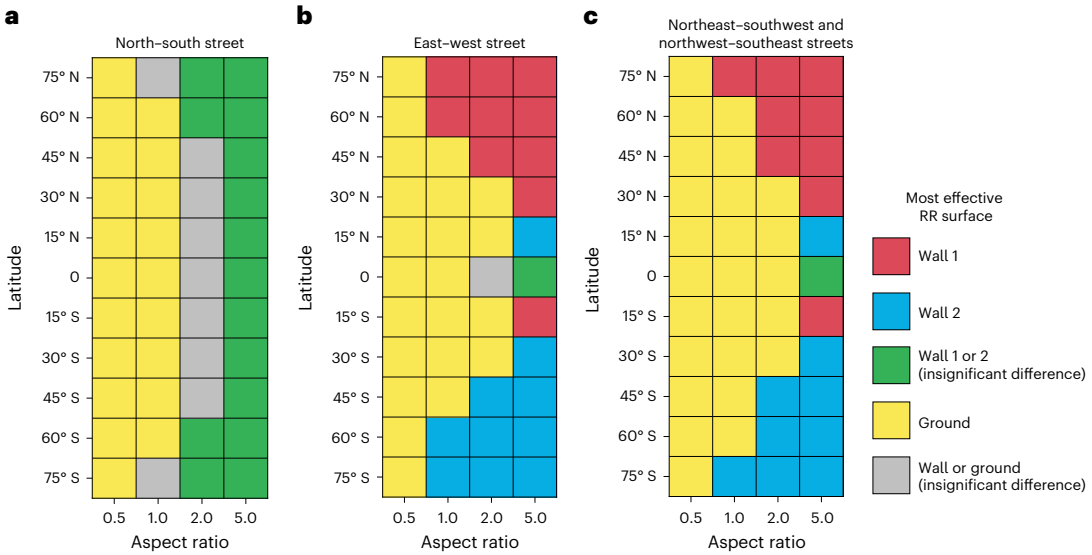

Fig. 6 | Optimization matrix of the most effective RR surfaces. a–c, Most effective RR surface to mitigate summertime extreme heat for different latitudes and aspect ratios in a north–south street (**a**), east–west street (**b**) and northeast–southwest or northwest–southeast street (**c**).

latitudinal and seasonal solar radiation variation). We found that RR surfaces outperform HR surfaces, especially in deep street canyons, with up to 3.1 °C additional canyon air temperature reduction. If only one urban facet is to be retrofitted considering cost-effectiveness, RR grounds are generally recommended for low-rise, low-density areas, especially at low latitudes, while RR walls become more effective with increasing latitude or canyon aspect ratio that represent high-rise, high-density areas. Synthesizing the above research findings, we provided an optimization matrix to illustrate the most effective RR surface for alleviating summertime extreme heat for global cities across latitudes and urban densities.

From evaluation to optimization, this study bridges the gaps between the innovative cooling concept of RR surfaces and the detailed practical blueprints needed for implementation, providing worldwide generalized design guidelines with informed cooling benefits as important references for material engineers, building designers, urban planners and policymakers. With greater applicability in diverse urban forms and superior cooling performances across latitudes, not only are RR surfaces an important improvement over HR surfaces but also they will be an indispensable element of the multi-technology cooling portfolios needed to tackle the exacerbating urban overheating problem.

It should be noted that the findings outlined in this paper are based on numerical simulations; translation to the real world will thus need to consider some uncertainties and caveats. For example, the present results represent an infinitely long canyon fully converted to RR surfaces; therefore, surface cooling will be moderately weaker and air cooling evidently weaker if only a section of a canyon is converted to an RR surface. Another factor to consider is cloud cover; since one of our primary research focuses is to mitigate extreme heat in sun-drenched cities, which are the most suitable application scenarios for RR surfaces, we used clear-sky radiation at all latitudes and focused on summer days in various analyses. The cooling potentials of RR surfaces would definitely be reduced during overcast periods and in cities. Thus, applying the model to a specific city with its specific meteorological conditions and urban morphology is needed to reduce uncertainty in the benefits of RR application for that specific location.

For future research, additional field observations are needed to better characterize the real-world benefits of RR façades. From a modeling perspective, a more comprehensive representation of angular distributions for various RR material types[20,21,23,44,45] could be incorporated into the existing model. This would allow a more nuanced assessment and modulation of the temporal patterns of their cooling effects: retro-reflectivity can be adjusted according to different incident angles and microscale structures to produce diurnally varying and seasonally varying retro-reflectivity profiles. For example, retro-reflectivity can peak in summer[22] and at noon[45] and diminish in winter and at night. Such patterns can potentially maximize cooling benefits during hotter periods and minimize cooling penalties during colder periods. Another useful extension of this research is to couple the PUCM to an atmospheric model[38,46,47] to evaluate the benefits of variable scales of implementation of RR façades over a city. Such coupling will allow the simulations to capture the feedback on air temperature above the canyon, which would boost the cooling benefits reported here for large-scale RR implementation. Lastly, the visual comfort benefits of RR surfaces, compared with HR ones, are essential but were not quantified in this study. The reduction in glare to pedestrians and drivers in the street canyon could also be evaluated when RR applications in cities are being considered.

Methods

Urban canopy model

The UCM framework is one of the most widely used land surface models for parameterizing surface–atmosphere exchanges of energy and water to reproduce micrometeorological conditions over built terrain, for example, in between buildings at the pedestrian level. Adopting the most common "big canyon" representation, the PUCM used in this study consists of two distinct facing walls, a ground and a roof. The PUCM considers radiative, turbulent and conductive energy exchanges among the facets and the air in or above the canyon. A unique feature of the PUCM is its ability to represent subfacet heterogeneity, such as grounds composed of a mix of asphalt, concrete and grass surfaces. The PUCM reproduces the heat fluxes and temperatures of each urban surface based on an urban surface energy budget (equation (1)) applied over an infinitesimally thin interface:

$$R = H + \mathrm{LE} + G \tag{1}$$

where R is the net all-wave radiation resolved by a two-reflection model, detailed in the following section; H and LE are turbulent sensible and latent heat fluxes, respectively, both parameterized by a resistance method[48] and the Monin–Obukhov similarity theory[49] considering canyon air heat capacity; G is the conductive heat flux resolved with

an analytical heat transfer approach using Green's function[50]. A bulk energy budget model is also applied to the canyon air, which has thermal mass and exchanges heat with the canyon facets and the air aloft (and is also potentially heated by anthropogenic sources). Here we underline that the canyon air temperature computed by the UCM is that of the air layers adjacent to the surfaces, and the cooling of the full air mass inside the canyon will be lower than the reported reductions. The PUCM has been successfully validated in various climates and seasons, showing robust capabilities to predict micrometeorological changes (for example, street canyon air temperature, T_{can}) induced by urban surface modification[35–37,46,51,52].

Furthermore, a human thermo-physiological model has been developed and coupled with the PUCM. It can predict human thermal comfort (represented by human skin temperature, T_{skin}) largely controlled by radiative shading and trapping (represented by net human radiation, R_{nh}) within detailed street canyon configurations[51]. The human model resolves the radiative, convective, conductive and evaporative heat exchanges between human bodies and surrounding environments by representing the body as a single mass cylinder with an outer skin interface that has negligible thermal inertia. For the skin surface, the governing energy balance equation is given as follows:

$$R_{nh} + C_h + E_h + K_h = 0 \tag{2}$$

where R_{nh} is the net human radiation, which is the sum of net (that is, incoming − outgoing) shortwave and longwave radiation from human bodies, given by $R_{nh} = SW_{in} - SW_{out} + LW_{in} - LW_{out}$; C_h and E_h are convective and evaporative heat exchanges, respectively, between human bodies and surrounding environments. K_h is the conductive exchange between the skin and the interior of the body, which is simulated as two thermal masses, an outer and a core one, with a thermal energy budget and accounting for metabolic heat generation in the core. The calculation method for each term has been detailed in our previous work[51]. Human skin temperature (T_{skin}) is calculated based on this equation (as a fourth-order polynomial for T_{skin}) and used to represent human thermal comfort levels in this study.

The PUCM can be coupled with an atmospheric model, such as WRF[38,46,47], or used "offline" driven by atmospheric observations or inputs. Offline applications, as used in this study, offer the ability to simulate various local environmental settings with low computational demands, allowing better analyses of problems with large parameter spaces for studying urban microclimatic responses to building surface changes. Thus, in this study, we choose the offline application of the UCM to investigate the impacts of RR surfaces in different street geometries and climatic conditions, leaving the possibility to further explore their broader impacts, considering regional land-use land-cover patterns, by coupling the developed PUCM-RR with meso- or global-scale atmospheric models in future studies.

Retro-reflective surface simulation

On the basis of the above-described PUCM, we developed a new radiation module that incorporates the effects of RR materials on the existing two-reflection radiation framework. In the previous PUCM, we solved radiative energy distribution and redistribution by considering two reflections between urban facets, assuming all urban surfaces to be Lambertian, that is, with isotropic scattering and reflection (Fig. 1a). To parametrize the RR feature, we need to incorporate and modify two important optical properties: total reflectivity and retro-reflectivity. The total reflectivity (α), also known as albedo, represents the ratio of reflected solar radiation to the total incoming solar radiation. Retro-reflectivity (η) represents the ratio of radiation reflected back at the same incident angle to the total reflected radiation, while the other fraction of radiation is assumed to be perfectly diffusely reflected. With a total incoming solar radiation of $S_{\downarrow}$, an RR surface will absorb $(1-\alpha)S_{\downarrow}$, retro-reflect $\alpha\eta S_{\downarrow}$ and diffusively reflect $\alpha(1-\eta)S_{\downarrow}$ (see Fig. 1c for schematic illustration). Note that in this study we adopt experimental reflectivity values for three common RR types from a review article[30] synthesizing 61 RR-related publications. RR surfaces do not retro-reflect all radiation in the same incident direction, but rather there is some variability in the exact retro-reflection angle, which we do not consider here. The detailed directional characteristics of the RR material we use have been parameterized in the bulk retro-reflectivity (η) based on these previous studies but not represented in detail. From the PUCM perspective, the exact retro-reflection angle is not crucial, and we mainly need to know the bulk fraction reflected to the sky (η) versus other urban facets.

To resolve shortwave radiation distribution among different urban surfaces, we first calculate direct and diffuse solar radiation distribution based on normalized shadow length and view factors, respectively. The total sky solar radiation, without considering any reflections for walls and ground, is given, respectively, as follows:

$$S_W^0 = S^d \frac{l_{shadow}}{2h} + S^q \frac{F_{WS}}{A_W} \tag{3}$$

$$S_G^0 = S^d \frac{w - l_{shadow}}{w} + S^q \frac{F_{GS}}{A_G} \tag{4}$$

where S_i^0 is the sum of direct and diffuse shortwave radiation on surface i from the sky, excluding any reflections, with subscripts W and G denoting walls and ground, respectively; S^d and S^q are direct and diffuse solar radiation (meteorological forcing), respectively; h, w and l_{shadow} are wall height, street width and shadow length normalized by the sum of street width and roof width, respectively[48,53]; F_{ij} is the view factor to surface i from surface j; A_i is the area of surface i relative to the canyon width.

Then, we consider radiation reflection up to two times inside the street canyon (all incident radiation is assumed to be absorbed in the third façade it impinges on). For walls and ground, we can calculate their net shortwave radiation as follows:

$$\begin{aligned} S_i^{net} &= (1-\alpha_i)S_i^0 \\ &+(1-\alpha_i)\sum_j^2 \alpha_j(1-\eta_j)S_j^0 \frac{A_j}{A_i}F_{ji} \\ &+\sum_j^2 \alpha_j(1-\eta_j)S_j^0 \sum_k^2 \frac{A_j}{A_k}F_{jk}\alpha_k \frac{A_k}{A_i}F_{ki} \end{aligned} \tag{5}$$

where S_i^{net} is the net shortwave radiation of surface i; α_i is the solar reflectivity (albedo) of surface i; η_j is the retro-reflectivity of surface j. The second line in equation (5) represents the first reflection, and the third line represents the second reflection. Note that for roofs, the shortwave radiation is resolved with one reflection that is not directly relevant to reflection properties inside the street canyon, that is, $S_R = (1-\alpha_R)(S^d + S^q)$. By contrast, RR roofs would not alter the canyon energy budget in a uniform urban area and are not studied here.

For an RR surface i, $(1-\alpha_i)$ represents the fraction of shortwave radiation absorbed by the RR surface, while $\alpha_i(1-\eta_i)$ represents the fraction of shortwave radiation reflected to the street canyon, with the other fraction ($\alpha_i\eta_i$) retro-reflected back to the radiation source (mostly back to the sky). Note that in the two-reflection model, retro-reflectivity (η_j) is always multiplied by view factors (F_{ji}, F_{jk}, F_{ki}) to reproduce different responses of in-canyon radiation exchanges to RR surface application under various urban dimensions and RR surface selection. Since the PUCM has been extensively validated before, and the RR radiation calculations proceed from first principles (energy conservation) given the imposed optical properties, there is no need for validating PUCM-RR, and there are, in fact, no datasets available for such validation at present. In addition, the longwave radiation properties of most RR materials are not much different from traditional materials, which

are broadband omnidirectional emitters, because these RR materials are usually inorganic dielectrics. Depending on the design, the exterior surface (for example, prism layer without any additional coating) can have low emissivity, which would then lead to longwave trapping. However, this possibility is not considered in our study since, as shown in Fig. 3, the indirect longwave radiation effect is much smaller than the direct shortwave untrapping. Thus, the longwave radiation calculation method (similarly using the two-reflection model[36,53]) remains unchanged, but the longwave radiation budget of each urban facet would be altered as a secondary impact considering reduced surface temperatures.

Numerical experiment design

As the use of RR material on building surfaces is a novel practice with limited documentation of UHI abatement effectiveness, we first evaluated its cooling effects with different total and retro-reflectivity, considering common RR material types implemented on walls and ground, and then further applied RR surfaces in various urban configurations (for example, different street geometries and orientations) and climatic conditions (for example, different latitudes and seasons) to explore their climate applicability and localized optimization.

The PUCM was driven by meteorological forcing data measured by a rooftop eddy-covariance tower during 2010–2011 on the Princeton University Campus in Princeton, NJ, USA[35,37]. The simulation was conducted to explore the hottest day (7 July 2010) during the 1-year meteorological measurement, with a 3-day spin-up period to provide realistic initial conditions and allow the walls and grounds to equilibrate. The important meteorological forcing, including atmospheric temperature, relative humidity, wind speed and downwelling shortwave radiation during the 4 days, is shown in Supplementary Fig. 2. As shown in Supplementary Fig. 2, these 4 days (4–7 July) are all hot and sunny, with a maximum air temperature of 39 °C at 16:00 on 7 July. The meteorological conditions are generally representative of extremely hot conditions with high air temperature, high air humidity and low wind speed. The shortwave radiation forcing shows fluctuations during the tested day due to intermittent clouds. Thus, in the simulation, we adopted an ideal clear-sky diurnal profile of solar radiation mainly based on Julian day and solar zenith angles[54] to more clearly observe the maximum cooling performance of RR surfaces by removing these confounding cloud impacts. Note that for the global solar radiation analysis, we only use the latitudinal, seasonal and diurnal information to generate ideal clear-sky solar radiation profiles for driving the UCM radiation module, so the tested street canyon shortwave radiation (S_{can}) is independent of differences in air temperature, humidity, wind, cloudiness and other meteorological factors among cities worldwide.

To evaluate the cooling benefits of RR material compared with normal material, we first set up a baseline scenario with normal (Lambertian) walls and ground with their typical albedos (0.25 and 0.15, respectively[55]). Other model input parameters, for example, latitude, canyon dimension and canyon orientation, were first set based on the local meteorological measurements (that is, at Princeton) in the baseline scenario and then modified to explore their individual impacts on RR cooling performance. Environmental properties and RR material properties for each scenario are presented in Supplementary Table 1, and other model parameters that are not explicitly addressed herein are identical to those described in ref. 35. As detailed in Supplementary Table 1, we use one representative wall energy budget for all simulations on 7 July and use two separate wall energy budgets to consider the optimal selection between different wall orientations in all other simulations.

Reporting summary

Further information on research design is available in the Nature Research Reporting Summary linked to this article.

Data availability

The simulation data for this study are available in the open-access Zenodo repository[56] at https://doi.org/10.5281/zenodo.10638146.

Code availability

The core MATLAB codes used for incorporating retro-reflectivity in shortwave radiation can be accessed via the open-access Zenodo repository[56] at https://doi.org/10.5281/zenodo.10638146. The whole UCM codes used in this study are available upon request from the corresponding author or X.H. (e-mail: xjhuang@princeton.edu).

References

1. Oke, T. R. The energetic basis of the urban heat island. *Q. J. R. Meteorol. Soc.* **108**, 1–24 (1982).
2. Santamouris, M. Recent progress on urban overheating and heat island research. Integrated assessment of the energy, environmental, vulnerability and health impact. Synergies with the global climate change. *Energy Build.* **207**, 109482 (2020).
3. Vicedo-Cabrera, A. M. et al. The burden of heat-related mortality attributable to recent human-induced climate change. *Nat. Clim. Change* **11**, 492–500 (2021).
4. Santamouris, M. Cooling the cities—a review of reflective and green roof mitigation technologies to fight heat island and improve comfort in urban environments. *Sol. Energy* **103**, 682–703 (2014).
5. Sen, S. & Khazanovich, L. Limited application of reflective surfaces can mitigate urban heat pollution. *Nat. Commun.* **12**, 3491 (2021).
6. Akbari, H. & Levinson, R. Evolution of cool-roof standards in the US. *Adv. Build. Energy Res.* **2**, 1–32 (2008).
7. Shultz, D. Los Angeles paints streets white to stay cool. *Science* https://www.science.org/content/article/los-angeles-paints-streets-white-stay-cool (2017).
8. Schneider, F. A., Ortiz, J. C., Vanos, J. K., Sailor, D. J. & Middel, A. Evidence-based guidance on reflective pavement for urban heat mitigation in Arizona. *Nat. Commun.* **14**, 1467 (2023).
9. Erell, E., Pearlmutter, D., Boneh, D. & Kutiel, P. B. Effect of high-albedo materials on pedestrian heat stress in urban street canyons. *Urban Clim.* **10**, 367–386 (2014).
10. Wang, C., Wang, Z.-H., Kaloush, K. E. & Shacat, J. Cool pavements for urban heat island mitigation: a synthetic review. *Renew. Sustain. Energy Rev.* **146**, 111171 (2021).
11. Yang, J. & Bou-Zeid, E. Scale dependence of the benefits and efficiency of green and cool roofs. *Landsc. Urban Plan.* **185**, 127–140 (2019).
12. Rossi, F. et al. Retroreflective façades for urban heat island mitigation: experimental investigation and energy evaluations. *Appl. Energy* **145**, 8–20 (2015).
13. Yuan, J., Emura, K., Farnham, C. & Sakai, H. Application of glass beads as retro-reflective facades for urban heat island mitigation: experimental investigation and simulation analysis. *Build. Environ.* **105**, 140–152 (2016).
14. Levinson, R. et al. Design, characterization, and fabrication of solar-retroreflective cool-wall materials. *Sol. Energy Mater. Sol. Cells* **206**, 110117 (2020).
15. Garshasbi, S. & Santamouris, M. Using advanced thermochromic technologies in the built environment: recent development and potential to decrease the energy consumption and fight urban overheating. *Sol. Energy Mater. Sol. Cells* **191**, 21–32 (2019).
16. Fabiani, C., Pisello, A. L., Bou-Zeid, E., Yang, J. & Cotana, F. Adaptive measures for mitigating urban heat islands: the potential of thermochromic materials to control roofing energy balance. *Appl. Energy* **247**, 155–170 (2019).
17. Mandal, J., Yang, Y., Yu, N. & Raman, A. P. Paints as a scalable and effective radiative cooling technology for buildings. *Joule* **4**, 1350–1356 (2020).

18. Yin, X., Yang, R., Tan, G. & Fan, S. Terrestrial radiative cooling: using the cold universe as a renewable and sustainable energy source. *Science* **370**, 786–791 (2020).
19. Castellani, B., Morini, E., Anderini, E., Filipponi, M. & Rossi, F. Development and characterization of retro-reflective colored tiles for advanced building skins. *Energy Build.* **154**, 513–522 (2017).
20. Liu, S., Wang, J. & Meng, X. Spectral properties of retro-reflective materials from experimental measurements. *Case Stud. Therm. Eng.* **39**, 102434 (2022).
21. Mauri, L., Battista, G., de Lieto Vollaro, E. & de Lieto Vollaro, R. Retroreflective materials for building's façades: experimental characterization and numerical simulations. *Sol. Energy* **171**, 150–156 (2018).
22. Akbari, H. & Touchaei, A. G. Modeling and labeling heterogeneous directional reflective roofing materials. *Sol. Energy Mater. Sol. Cells* **124**, 192–210 (2014).
23. Manni, M., Lobaccaro, G., Goia, F. & Nicolini, A. An inverse approach to identify selective angular properties of retro-reflective materials for urban heat island mitigation. *Sol. Energy* **176**, 194–210 (2018).
24. Rossi, F. et al. Experimental evaluation of urban heat island mitigation potential of retro-reflective pavement in urban canyons. *Energy Build.* **126**, 340–352 (2016).
25. Ichinose, M., Inoue, T. & Nagahama, T. Effect of retro-reflecting transparent window on anthropogenic urban heat balance. *Energy Build.* **157**, 157–165 (2017).
26. Han, Y., Taylor, J. E. & Pisello, A. L. Toward mitigating urban heat island effects: investigating the thermal-energy impact of bio-inspired retro-reflective building envelopes in dense urban settings. *Energy Build.* **102**, 380–389 (2015).
27. Meng, X. et al. Effect of retro-reflective materials on building indoor temperature conditions and heat flow analysis for walls. *Energy Build.* **127**, 488–498 (2016).
28. Castellani, B., Gambelli, A. M., Nicolini, A. & Rossi, F. Optic-energy and visual comfort analysis of retro-reflective building plasters. *Build. Environ.* **174**, 106781 (2020).
29. Xu, L., Zhang, W., Wang, W., Gao, B. & Chen, M. Impact of different improvement measures on the thermal performance of ultra-thin envelopes. *Energy* **203**, 117802 (2020).
30. Wang, J., Liu, S., Meng, X., Gao, W. & Yuan, J. Application of retro-reflective materials in urban buildings: a comprehensive review. *Energy Build.* **247**, 111137 (2021).
31. Lipson, M. J. et al. Evaluation of 30 urban land surface models in the Urban-PLUMBER project: phase 1 results. *Q. J. R. Meteorol. Soc.* **150**, 126–169 (2024).
32. Grimmond, C. S. B. et al. The international urban energy balance models comparison project: first results from phase 1. *J. Appl. Meteorol. Climatol.* **49**, 1268–1292 (2010).
33. Grimmond, C. S. B. et al. Initial results from phase 2 of the international urban energy balance model comparison. *Int. J. Climatol.* **31**, 244–272 (2011).
34. Oleson, K. W. & Feddema, J. Parameterization and surface data improvements and new capabilities for the community land model urban (CLMU). *J. Adv. Model. Earth Syst.* **12**, e2018MS001586 (2020).
35. Wang, Z.-H., Bou-Zeid, E. & Smith, J. A. A coupled energy transport and hydrological model for urban canopies evaluated using a wireless sensor network. *Q. J. R. Meteorol. Soc.* **139**, 1643–1657 (2013).
36. Ryu, Y.-H., Bou-Zeid, E., Wang, Z.-H. & Smith, J. A. Realistic representation of trees in an urban canopy model. *Bound. Layer Meteorol.* **159**, 193–220 (2016).
37. Sun, T., Bou-Zeid, E., Wang, Z.-H., Zerba, E. & Ni, G.-H. Hydrometeorological determinants of green roof performance via a vertically-resolved model for heat and water transport. *Build. Environ.* **60**, 211–224 (2013).
38. Li, D. & Bou-Zeid, E. Quality and sensitivity of high-resolution numerical simulation of urban heat islands. *Environ. Res. Lett.* **9**, 055001 (2014).
39. Ramamurthy, P. et al. Influence of subfacet heterogeneity and material properties on the urban surface energy budget. *J. Appl. Meteorol. Climatol.* **53**, 2114–2129 (2014).
40. Yuan, J., Farnham, C. & Emura, K. Development of a retro-reflective material as building coating and evaluation on albedo of urban canyons and building heat loads. *Energy Build.* **103**, 107–117 (2015).
41. Sakai, H., Kobayashi, H., Emura, K. & Igawa, N. Outdoor measurement of solar reflective performance of retroreflective materials. *J. Struct. Constr. Eng.* **73**, 1713–1718 (2008).
42. Sakai, H., Emura, K. & Igawa, N. Reduction of reflected heat by retroreflective materials. *J. Struct. Constr. Eng.* **73**, 1239–1244 (2008).
43. Hagander, L. G., Midani, H. A., Kuskowski, M. A. & Parry, G. J. G. Quantitative sensory testing: effect of site and skin temperature on thermal thresholds. *Clin. Neurophysiol.* **111**, 17–22 (2000).
44. Rossi, F., Pisello, A. L., Nicolini, A., Filipponi, M. & Palombo, M. Analysis of retro-reflective surfaces for urban heat island mitigation: a new analytical model. *Appl. Energy* **114**, 621–631 (2014).
45. Yuan, J., Emura, K. & Farnham, C. Evaluation of retro-reflective properties and upward to downward reflection ratio of glass bead retro-reflective material using a numerical model. *Urban Clim.* **36**, 100774 (2021).
46. Ramamurthy, P. & Bou-Zeid, E. Heatwaves and urban heat islands: a comparative analysis of multiple cities. *J. Geophys. Res. Atmos.* **122**, 168–178 (2017).
47. Yang, J. & Bou-Zeid, E. Should cities embrace their heat islands as shields from extreme cold? *J. Appl. Meteorol. Climatol.* **57**, 1309–1320 (2018).
48. Masson, V. A physically-based scheme for the urban energy budget in atmospheric models. *Bound. Layer Meteorol.* **94**, 357–397 (2000).
49. Song, Y. An improvement of the Louis scheme for the surface layer in an atmospheric modelling system. *Bound. Layer Meteorol.* **88**, 239–254 (1998).
50. Wang, Z.-H., Bou-Zeid, E. & Smith, J. A. A spatially-analytical scheme for surface temperatures and conductive heat fluxes in urban canopy models. *Bound. Layer Meteorol.* **138**, 171–193 (2011).
51. Pigliautile, I., Pisello, A. L. & Bou-Zeid, E. Humans in the city: representing outdoor thermal comfort in urban canopy models. *Renew. Sustain. Energy Rev.* **133**, 110103 (2020).
52. Li, D., Bou-Zeid, E. & Oppenheimer, M. The effectiveness of cool and green roofs as urban heat island mitigation strategies. *Environ. Res. Lett.* **9**, 055002 (2014).
53. Kusaka, H., Kondo, H., Kikegawa, Y. & Kimura, F. A simple single-layer urban canopy model for atmospheric models: comparison with multi-layer and slab models. *Bound. Layer Meteorol.* **101**, 329–358 (2001).
54. Daneshyar, M. Solar radiation statistics for Iran. *Sol. Energy* **21**, 345–349 (1978).
55. *2009 ASHRAE Handbook: Fundamentals* (American Society of Heating, Refrigeration and Air-Conditioning Engineers, 2009).
56. Huang, X. Data and code for retro-reflective surface paper. *Zenodo* https://doi.org/10.5281/zenodo.10638146 (2024).

Acknowledgments

X.H. and E.B.-Z. acknowledge support from Princeton University's School of Engineering Innovation Funds and the Dean of Research Innovation Fund for Exploratory Energy Research. A.L.P. thanks the European Research Council for supporting her research in the framework of the Horizon Europe Programme (ERC, HELIOS,

G.A. 101041255). I.P. thanks the Italian funding program Fondo Sociale Europeo REACT EU – Programma Operativo Nazionale Ricerca e Innovazione 2014–2020 (D.M. n.1062 del 10 agosto 2021) for supporting her research through the "Red-To-Green" project. J.M. acknowledges support from Princeton University's SEAS start-up funds.

Author contributions

X.H. and E.B.-Z. designed the methodology and scientific questions. E.B.-Z. and A.L.P. conceived the idea of using RR materials for cooling. X.H. developed the RR model, and I.P. developed the human thermal comfort model. X.H. analyzed and visualized the data. J.M. contributed to refining the methodology and presentation. X.H. and E.B.-Z. led the writing. All authors contributed to the writing and presentation of the results and gave final approval for publication.

Competing interests

The authors declare no competing interests.

Additional information

Supplementary information The online version contains supplementary material available at https://doi.org/10.1038/s44284-024-00047-3.

Correspondence and requests for materials should be addressed to Elie Bou-Zeid.

Peer review information *Nature Cities* thanks Mattia Manni, Chaoqun Zhuang and the other, anonymous, reviewer(s) for their contribution to the peer review of this work.

nature portfolio

Corresponding author(s): Elie Bou-Zeid

Last updated by author(s): Feb 9, 2024

Reporting Summary

Nature Portfolio wishes to improve the reproducibility of the work that we publish. This form provides structure for consistency and transparency in reporting. For further information on Nature Portfolio policies, see our Editorial Policies and the Editorial Policy Checklist.

Statistics

For all statistical analyses, confirm that the following items are present in the figure legend, table legend, main text, or Methods section.

n/a	Confirmed	
☒	☐	The exact sample size (*n*) for each experimental group/condition, given as a discrete number and unit of measurement
☒	☐	A statement on whether measurements were taken from distinct samples or whether the same sample was measured repeatedly
☒	☐	The statistical test(s) used AND whether they are one- or two-sided *Only common tests should be described solely by name; describe more complex techniques in the Methods section.*
☒	☐	A description of all covariates tested
☒	☐	A description of any assumptions or corrections, such as tests of normality and adjustment for multiple comparisons
☒	☐	A full description of the statistical parameters including central tendency (e.g. means) or other basic estimates (e.g. regression coefficient) AND variation (e.g. standard deviation) or associated estimates of uncertainty (e.g. confidence intervals)
☒	☐	For null hypothesis testing, the test statistic (e.g. *F*, *t*, *r*) with confidence intervals, effect sizes, degrees of freedom and *P* value noted *Give P values as exact values whenever suitable.*
☒	☐	For Bayesian analysis, information on the choice of priors and Markov chain Monte Carlo settings
☒	☐	For hierarchical and complex designs, identification of the appropriate level for tests and full reporting of outcomes
☒	☐	Estimates of effect sizes (e.g. Cohen's *d*, Pearson's *r*), indicating how they were calculated

Our web collection on statistics for biologists contains articles on many of the points above.

Software and code

Policy information about availability of computer code

Data collection	No software was used for data collection.
Data analysis	The custom codes can be publicly accessed in a Zenodo repository: https://doi.org/10.5281/zenodo.10638146.

For manuscripts utilizing custom algorithms or software that are central to the research but not yet described in published literature, software must be made available to editors and reviewers. We strongly encourage code deposition in a community repository (e.g. GitHub). See the Nature Portfolio guidelines for submitting code & software for further information.

Data

Policy information about availability of data

All manuscripts must include a data availability statement. This statement should provide the following information, where applicable:

- Accession codes, unique identifiers, or web links for publicly available datasets
- A description of any restrictions on data availability
- For clinical datasets or third party data, please ensure that the statement adheres to our policy

The simulation data in this study can be publicly accessed in a Zenodo repository: https://doi.org/10.5281/zenodo.10638146.

Research involving human participants, their data, or biological material

Policy information about studies with human participants or human data. See also policy information about sex, gender (identity/presentation), and sexual orientation and race, ethnicity and racism.

Reporting on sex and gender	Our research does not involve human participants.
Reporting on race, ethnicity, or other socially relevant groupings	Our research does not involve human participants.
Population characteristics	Our research does not involve human participants.
Recruitment	Our research does not involve human participants.
Ethics oversight	Our research does not involve human participants.

Note that full information on the approval of the study protocol must also be provided in the manuscript.

Field-specific reporting

Please select the one below that is the best fit for your research. If you are not sure, read the appropriate sections before making your selection.

☐ Life sciences ☐ Behavioural & social sciences ☒ Ecological, evolutionary & environmental sciences

For a reference copy of the document with all sections, see nature.com/documents/nr-reporting-summary-flat.pdf

Ecological, evolutionary & environmental sciences study design

All studies must disclose on these points even when the disclosure is negative.

Study description	This study employs the Princeton Urban Canopy Model (PUCM) to examine the effects of retro-reflective (RR) surfaces on urban microclimate and assesses their cooling impact in different urban configurations and climatic conditions.
Research sample	The research sample consists of data collected from meteorological measurements taken at Princeton University Campus in 2010-2011, primarily focusing on the hottest day (July 7th, 2010) to investigate the worst case, i.e., highest heat stress. The simulation has a three-day spin-up period to provide realistic initial conditions and allow the walls and grounds to equilibrate.
Sampling strategy	The PUCM was driven by meteorological forcing data measured by a rooftop eddy-covariance tower during 2010-2011 on the Princeton University Campus, NJ, U.S.. The simulation was conducted to explore the hottest day (July 7th, 2010) during the one-year meteorological measurement.
Data collection	Data is collected from a rooftop eddy-covariance tower and includes atmospheric temperature, relative humidity, wind speed, and downwelling shortwave radiation during the four-day period.
Timing and spatial scale	The study examines meteorological conditions on a hot period (July 4-7th, 2010) and considers variations in latitudinal, seasonal, and diurnal factors to evaluate RR surface performance within different street canyon settings.
Data exclusions	No data is excluded from this study, except for data during three spin-up days as they are to equilibrate initial conditions and not been studied.
Reproducibility	The numerical experiments can be reproduced with the same input data and same PUCM codes.
Randomization	Randomization is not relevant to our study as we conducted numerical experiments and then analyzed all the data, instead of using a statistical analysis method.
Blinding	Blinding in not relevant to our study as the study does not involve concealment of group allocation.

Did the study involve field work? ☐ Yes ☒ No

Reporting for specific materials, systems and methods

We require information from authors about some types of materials, experimental systems and methods used in many studies. Here, indicate whether each material, system or method listed is relevant to your study. If you are not sure if a list item applies to your research, read the appropriate section before selecting a response.

Materials & experimental systems

n/a	Involved in the study
☒	☐ Antibodies
☒	☐ Eukaryotic cell lines
☒	☐ Palaeontology and archaeology
☒	☐ Animals and other organisms
☒	☐ Clinical data
☒	☐ Dual use research of concern
☒	☐ Plants

Methods

n/a	Involved in the study
☒	☐ ChIP-seq
☒	☐ Flow cytometry
☒	☐ MRI-based neuroimaging

Plants

Seed stocks	This study does not involve any plants.
Novel plant genotypes	This study does not involve any plants.
Authentication	This study does not involve any plants.